Available online at www.sciencedirect.com

ScienceDirect

Ceramics International 40 (2014) 4869–4873

CERAMICS INTERNATIONAL

www.elsevier.com/locate/ceramint

Fabrication and characterization of $Zn_xCd_{1-x}S$ nanoparticles in chitosan alginate nanocomposite films

Liping Wang*, Yujie Sun, Xiaofei Yang

Department of Materials Physics and Chemistry, School of Materials Science and Engineering, University of Science and Technology Beijing, Beijing 100083, PR China

Received 23 August 2013; received in revised form 6 September 2013; accepted 7 September 2013
Available online 16 September 2013

Abstract

$Zn_xCd_{1-x}S$ nanoparticles were formed in chitosan alginate nanocomposite films using spin-coating technique. Crystal structure and size, optical properties and surface morphology were characterized by X-ray diffraction (XRD), ultraviolet–visible (UV–vis), photoluminescence (PL) spectra, transmission electron microscopy (TEM) and atomic force microscopy (AFM), respectively. The $Zn_xCd_{1-x}S$ nanoparticles have a cubic structure with an average crystal size of ~2 nm. With increasing Zn/Cd molar ratio, the UV–vis absorption peaks shift to low-wavelength side with a slight intensity decrease. The relative emission intensity of the film may be changed regularly by variation of the $Zn_xCd_{1-x}S$ nanoparticles composition. Surface morphology of the films containing $Zn_xCd_{1-x}S$ nanoparticles changes with various Zn/Cd molar ratios. The film morphology goes from rough to smooth with increasing Zn/Cd, and the phase goes from bump-like shape to particle-like shape with a more uniform distribution due to the radius difference between Zn and Cd ions.

Keywords: $Zn_xCd_{1-x}S$ nanoparticles; Nanocomposite films; Chitosan; Surface morphology

1. Introduction

Nanostructured semiconductors have attracted considerable interest to many research fields due to their special spectroscopic, electronic, and chemical properties compared to bulk materials and have applications in optoelectronics, solar photovoltaic devices, and chemical/biological sensors [1,2]. Among these applications, the band gap energy of a nanostructured semiconductor plays an important role [3,4]. One successful way of tuning the band gap is the combination of different semiconductors to form alloyed semiconductors on account of the band gap dependence on compositions [5]. Alloyed semiconductor nanomaterials have potential applications for the design of new devices, such as electronic devices, light-emitting diodes, biological labels, and catalysts [6–8]. ZnS and CdS are the most extensively studied and widely used II–VI semiconductors having a band gap of 3.68 and 2.49 eV, respectively [9,10]. Alloyed semiconductor $Zn_xCd_{1-x}S$ has a continuous tunable band gap between those of ZnS and CdS owing to the mutual substitution of metal ions in lattices [11–13]. Structural and optical properties of colloid $Zn_xCd_{1-x}S$ nanocrystals have been investigated [14–16]. However, few reports are available on the fabrication of alloyed $Zn_xCd_{1-x}S$ in biomacromolecule composite films.

Chitosan is a natural biomacromolecule obtained by the deacetylation of chitin and has been used in biological applications due to its favorable properties of good biocompatibility and low toxicity [17]. Alginate is also a natural biomacromolecule extracted from brown algea [18]. Positively charged chitosan and negatively charged alginate can form polyelectrolyte complexes and they are suitable for composite films owing to good film-forming abilities [19]. Furthermore, structural properties may make chitosan and alginate as favorable materials for composite films. The amino and hydroxyl groups in chitosan can chelate with metal ions, and the hydroxyl and carboxylic groups in alginate may also complex with metal ions, which results in the formation of

*Corresponding author. Tel./fax: +86 10 62334505.
E-mail address: lpwang@mater.ustb.edu.cn (L. Wang).

0272-8842/$ - see front matter © 2013 Elsevier Ltd and Techna Group S.r.l. All rights reserved.
http://dx.doi.org/10.1016/j.ceramint.2013.09.036

semiconductor nanocrystals and may provide a good opportunity for bioapplications [20,21].

In the present work, $Zn_xCd_{1-x}S$ nanoparticles were formed during the fabrication of chitosan alginate nanocomposite films via a simple spin-coating technique. Crystal structures and size of the $Zn_xCd_{1-x}S$ nanoparticles were characterized by X-ray diffraction spectroscopy and TEM. Moreover, optical properties and surface morphology of the composite films with various Zn/Cd molar ratios were investigated.

2. Experimental

Analytical grade reagents, zinc acetate, cadmium acetate, sodium sulfide, acetic acid, chitosan, and sodium alginate, were purchased from the local chemical manufacturer (Sinopharm Chemical Reagent Co. Ltd., China) and were used without further purification.

Chitosan and alginate solutions were prepared as follows. A metal-ion-containing chitosan solution was prepared by firstly adding 0.5 g of chitosan, zinc acetate and cadmium acetate with an appropriate molar ratio into 50 mL of deionized water, and then adding 1 mL of acetic acid and stirred for 2 h. A sulfur-ion-containing alginate solution was prepared by adding 0.5 g of alginate and 2.5 mmol of sodium sulfide into 50 mL of deionized water with stirring for 3 h. An alkaline alginate solution was prepared by adding 2.5 g of alginate into 50 mL of deionized water with stirring for 2 h, and then adding ammonia until the pH of the solution is 14 and stirring for 1 h.

A certain amount of the chitosan solution was transferred to a clean quartz substrate, and spin-coated for 30 min. The quartz substrate was then dried in an oven at 100 °C for 10 min to form a chitosan layer. Subsequently, the same quartz substrate was covered with a certain amount of the sulfur-ion-containing alginate solution and spin-coated and dried similarly as the above. As a result, $Zn_xCd_{1-x}S$ nanoparticles formed in between the chitosan and alginate layers. The preparation cycle was repeated to obtain more $Zn_xCd_{1-x}S$ nanoparticles in the polymer layers.

To characterize the phase structure of the $Zn_xCd_{1-x}S$ nanoparticles, XRD analysis was carried out using a D/max-RB X-ray diffractometer (Rigaku Corporation). To observe the size and morphology of the $Zn_xCd_{1-x}S$ nanoparticles, a FEI-F20 transmission electron microscopy (FEI Co.) was used. To verify the composition of the nanoparticles, energy dispersive spectroscopy (EDS) was carried out on EDAX. To characterize surface morphology and optical properties of the composite films, atomic force microscopy, UV–visible absorption spectra and photoluminescence (PL) emission spectra was measured using a Nanoscope IIIa (Veeco), JASCO V570 UV spectrophotometer (Japan spectrophotometric instruments), and Hitachi F-4500 fluorescence spectrophotometer, respectively.

3. Results and discussion

The X-ray diffraction (XRD) pattern of $Zn_xCd_{1-x}S$/chitosan/alginate nanocomposite films is shown in Fig. 1. For the sample with a molar ratio of Zn/Cd = 9:1, the diffraction peaks

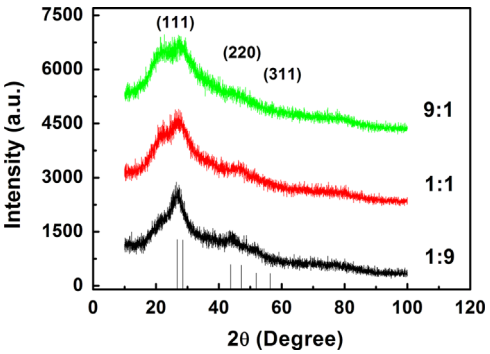

Fig. 1. The XRD patterns of $Zn_xCd_{1-x}S$ nanoparticles in chitosan/alginate composite films with a Zn/Cd molar ratio of 1:9, 1:1, and 9:1.

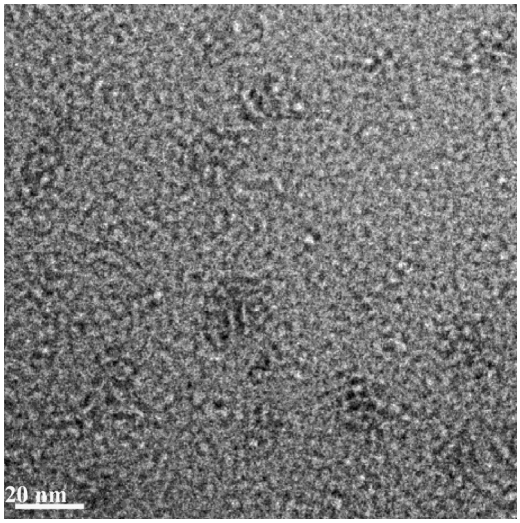

Fig. 2. Typical TEM image for the $Zn_xCd_{1-x}S$/chitosan/alginate composite film with a Zn/Cd molar ratio of 1:1.

can be indexed to standard cubic ZnS (JCPDS no. 05-0566), which is shown as the vertical lines along the axis of two theta. The mean crystalline size is calculated to be ~2 nm, using the well-known Scherrer equation, $D = k\lambda/\beta \cos \theta$. For the sample with a molar ratio of Zn/Cd = 1:9, the diffraction peaks can be indexed to standard cubic CdS (JCPDS no. 89-0440), which is shown as the vertical lines with asterisk along the axis of two theta. While for the sample with a Zn/Cd molar ratio of 1:1, the peak position is in between the standard ZnS and CdS. The results demonstrate the formation of cubic $Zn_xCd_{1-x}S$ nanoparticles in the composite films, although the curves are a little blur due to the presence of polymers.

Fig. 2 shows a typical TEM image for the $Zn_xCd_{1-x}S$/chitosan/alginate nanocomposite film containing equal molar of Zn and Cd. The $Zn_xCd_{1-x}S$ nanoparticles are quite small and uniformly distributed in the film. The size of the $Zn_xCd_{1-x}S$ nanoparticles is ~2 nm, which is in good agreement with what obtained from the XRD analysis.

Fig. 3 shows the ultraviolet–visible (UV–vis) absorption spectra of the $Zn_xCd_{1-x}S$/chitosan/alginate nanocomposite films with different Zn/Cd ratios. The curves are similar in shape and have an absorption in the range of 290–360 nm.

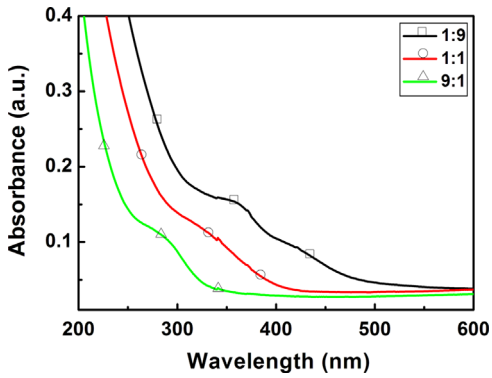

Fig. 3. UV–vis absorption spectra of $Zn_xCd_{1-x}S$ nanoparticles in chitosan/alginate composite films with a Zn/Cd molar ratio of 1:9, 1:1, and 9:1.

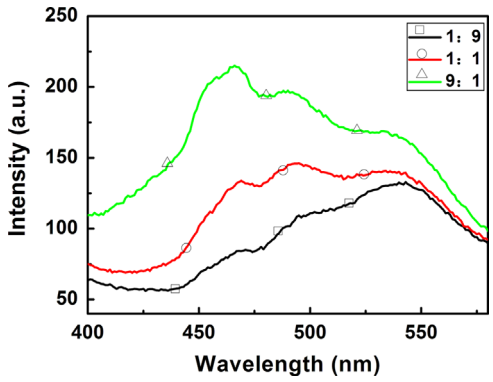

Fig. 4. Emission spectra of $Zn_xCd_{1-x}S$ nanoparticles in chitosan/alginate composite films with a Zn/Cd molar ratio of 1:9, 1:1, and 9:1.

Table 1
UV–vis absorption and band gap value for the $Zn_xCd_{1-x}S$/chitosan/alginate films with various Zn/Cd molar ratios.

Zn/Cd molar ratio	Absorption peak (nm)	Absorption intensity	Band gap value (eV)
1:9	357.36	0.154	3.47
1:4	346.36	0.145	3.58
3:7	333.12	0.141	3.72
2:3	320.56	0.132	3.87
1:1	318.76	0.123	3.89
3:2	301.27	0.117	4.12
7:3	300.14	0.114	4.13
4:1	297.22	0.112	4.17
9:1	290.26	0.106	4.27

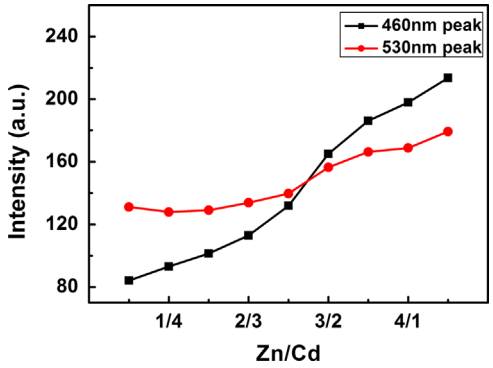

Fig. 5. Variation of UV–vis absorption intensity for the peaks at 460, and 530 nm versus Zn/Cd molar ratio for the composite films.

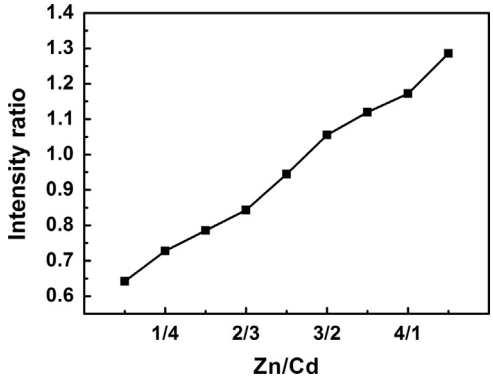

Fig. 6. UV–vis absorption intensity ratio for the peaks at 460, and 530 nm versus Zn/Cd molar ratio for the composite films.

For the sample with a Zn/Cd molar ratio of 9:1, the absorption peak locates at around 290 nm, which is significantly blue-shifted compared to that for bulk ZnS (340 nm). For the sample with a Zn/Cd molar ratio of 1:9, the absorption peak locates at around 360 nm, which is also blue-shifted compared to that for bulk CdS (515 nm). For the sample with equal molar of Zn and Cd, the absorption peak is in between 290 and 360 nm. The result suggests that the $Zn_xCd_{1-x}S$ nanoparticles show quantum effect due to their small size. Further studies for the samples with various Zn/Cd molar ratios were carried out, and the UV–vis data are shown in Table 1. The result implies the formation of $Zn_xCd_{1-x}S$ nanoparticles, because a mixture of pure ZnS and CdS nanoparticles could not lead to band gap intermediate to those of ZnS and CdS [22]. The result also shows that with increasing Zn/Cd molar ratio, the absorption peak shifts to low-wavelength side, the absorption intensity decreases slightly, and the band gap value increases. This may be due to the difference in ionic radius of Zn and Cd, as it is well known that the ionic radius of Cd is larger than that of Zn. The increase in Zn/Cd molar ratio will result in the increase of lattice and size for the $Zn_xCd_{1-x}S$ nanoparticles and a blue shift in absorption [5].

Fig. 4 shows the photoluminescent emission spectra of the $Zn_xCd_{1-x}S$ nanoparticles in the chitosan alginate films irradiated with the excitation light wavelength of 319 nm. There are three broad emission located at around 460, 490, and 530 nm. The emission around 490 nm is ascribed to the one from the chitosan and alginate film, and the emission around 460 and 530 nm comes from the $Zn_xCd_{1-x}S$ nanoparticles. The emission at around 460 nm can be attributed to the ZnS host and dopant metal ions [23]. The emission at around 530 nm can be ascribed to surface trap from CdS and dopant metal ions. Moreover, the dopant in ZnS lattice gives rise to the 530 nm emission. The emission peak position almost keeps

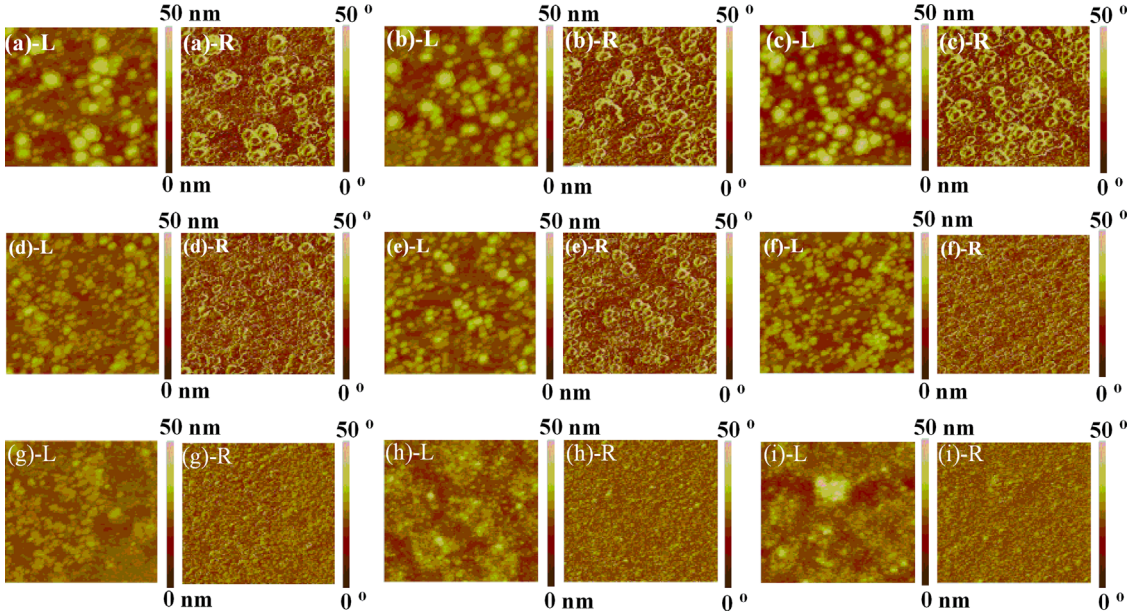

Fig. 7. AFM images of the $Zn_xCd_{1-x}S$/chitosan/alginate nanocomposite films with various Zn/Cd molar ratios. The (a)–(i) images are for the samples with a Zn/Cd molar ratio of 1:9, 1:4, 2:3, 3:7, 1:1, 7:3, 3:2, 4:1, and 1:9, respectively. For each sample, the left image represents the height of the film, and the right one represents the phase distribution of the film.

constant with various Zn/Cd molar ratios, suggesting that the emission mechanism does not change with different composition. However, the relative intensity changes with various Zn/Cd molar ratios. Further studies were carried out for the samples with a Zn/Cd molar ratio in the range from 1:9 to 9:1, and the results are shown in Figs. 5 and 6. It is obvious that both the 460 and 530 nm peak intensities increase with increasing Zn/Cd molar ratio. In addition, the intensity increase for the 460 nm peak is larger than that for the 530 nm peak, which is shown in Fig. 6, as a linear intensity ratio increase for the 460 and 530 nm peaks with increasing Zn/Cd molar ratio. This can be ascribed to the formation of $Zn_xCd_{1-x}S$ nanoparticles in the film. The relative emission intensity of the film may be changed regularly by variation of the $Zn_xCd_{1-x}S$ nanoparticles composition.

Atomic force microscopy was carried out in order to characterize the surface morphology of the nanocomposite films. Fig. 7 shows the AFM images of the $Zn_xCd_{1-x}S$/chitosan/alginate nanocomposite films with various Zn/Cd molar ratios. As a whole, the surface morphology of the composite films goes from rough to smooth with increasing Zn/Cd molar ratio, and the phase goes from bump-like shape to particle-like shape with a uniform distribution. When the Zn/Cd molar ratio is $\leq$1:4, the average height difference of the composite film is around 200 nm with a maximum of almost 300 nm. The surface of the composite films is quite rough with many bump-shaped phase, whose size is around 50 nm composed of a 10–20 nm particle-like low-sized phase surrounded with a 40 nm loop-shaped large-sized phase. The height difference of the films decreases with increasing Zn/Cd molar ratio. When the Zn/Cd molar ratio is 1:1, the average height difference is around 150 nm with a maximum of 200 nm. When the Zn/Cd molar ratio is $\geq$7:3, the height difference decreases and the averaged height is 70–80 nm with a maximum of 100 nm. The surface of the film looks smooth with almost no obvious phase boundary. When the Zn/Cd molar ratio is 9:1, the height difference is the lowest, and the average height is 25 nm with a maximum of around 50 nm. The surface of the film is smoother with low-sized phases uniformly distributed, whose size is 20–30 nm. The results suggest that the low-sized phase contains of more Zn and the large-sized loop-shaped phase contains of more Cd due to the radius difference between Zn and Cd ions. When the Zn ratio is larger, the film will be smoother with more low-sized phase.

4. Conclusions

$Zn_xCd_{1-x}S$ nanoparticles with cubic ZnS structure were synthesized in chitosan alginate nanocomposite films using spin-coating method. The band gap of the $Zn_xCd_{1-x}S$ nanoparticles can be tuned by adjusting the stoichiometry of Zn and Cd. Obvious blue shift in UV–vis absorption was observed due to small size effect. The absorption peak changes with the composition of $Zn_xCd_{1-x}S$ nanoparticles. Furthermore, the surface morphology of the composite films changes with the composition of $Zn_xCd_{1-x}S$ nanoparticles. With increasing Zn/Cd molar ratio, the film becomes smoother with more low-sized phase containing more Zn ions.

Acknowledgments

The authors gratefully acknowledge financial support from the National Science Foundation of China (Grant no. 21073012 and 20773012).

References

[1] Z.T. Deng, H. Yan, Y. Liu, Band gap engineering of quaternary-alloyed ZnCdSSe quantum dots via a facile phosphine-free colloidal method, Journal of the American Chemical Society 131 (2009) 17744–17745.

[2] C. Harris, P.V. Kamat, Photocatalytic events of CdSe quantum dots in confined media. Electrodic behavior of coupled platinum nanoparticles, ACS Nano 4 (2010) 7321–7330.

[3] E.M. Chan, R.A. Mathies, A.P. Alivisatos, Size-controlled growth of CdSe nanocrystals in microfluidic reactors, Nano Letter 3 (2003) 199–201.

[4] M.J. Li, J.Y. Ouyang, C.I. Ratcliffe, L. Pietri, X.H. Wu, D.M. Leek, I. Moudrakovski, Q. Lin, B. Yang, K. Yu, CdS magic-sized nanocrystals exhibiting bright band gap photoemission via thermodynamically driven formation, ACS Nano 3 (2009) 3832–3838.

[5] M.R. Kim, S.-Y. Park, D.-J. Jang, Composition variation and thermal treatment of $Zn_xCd_{1-x}S$ alloy nanoparticles to exhibit controlled and efficient luminescence, Journal of Physical Chemistry C 114 (2010) 6452–6457.

[6] Y.K. Liu, J.A. Zapien, Y.Y. Shan, C.Y. Geng, C.S. Lee, S.T. Lee, Wavelength-controlled lasing in $Zn_xCd_{1-x}S$ single-crystal nanoribbons, Advanced Materials 17 (2005) 1372–1377.

[7] W.L. Ma, J.M. Luther, H.M. Zheng, Y. Wu, A.P. Alivisatos, Photovoltaic devices employing ternary PbS_xSe_{1-x} nanocrystals, Nano Letter 9 (2009) 1699–1703.

[8] A.L. Pan, W.C. Zhou, E.S.P. Leong, R.B. Liu, A.H. Chin, B.S. Zou, C. Z. Ning, Continuous alloy-composition spatial grading and superbroad wavelength-tunable nanowire lasers on a single chip, Nano Letter 9 (2009) 784–788.

[9] S.H. Choi, K. An, E.G. Kim, J.H. Yu, J.H. Kim, T. Hyeon, Simple and generalized synthesis of semicoducting metal sulfide nanocrystals, Advanced Functional Materials 19 (2009) 1645–1649.

[10] X.H. Zhong, Y.Y. Feng, W. Knoll, M.Y. Han, Alloyed $Zn_xCd_{1-x}S$ nanocrystals with highly narrow luminescence spectral width, Journal of the American Chemical Society 125 (2003) 13559–13563.

[11] V.A. Fedorov, V.A. Ganshing, Y.U.N. Norkeshko, Solid-state phase diagram of the zinc sulfide–cadmium sulfide system, Materials Research Bulletin 28 (1993) 59–66.

[12] T.L. Chu, S.S. Chu, J. Britt, C. Ferekides, C.Q. Wu, Cadmium zinc sulfide films and heterojunctions, Journal of Applied Physics 70 (1991) 2688–2693.

[13] A. Nayeem, K. Yandaiah, G. Vajralingam, P. Mahesh, M. Nagabhooshanam, Synthesis and characterization of $Cd_{1-x}Zn_xS$:Cu crystals by co-precipitation method, International Journal of Modern Physics B 15 (2001) 2387–2407.

[14] X. Zhong, Y. Feng, W. Knoll, M. Hang, Alloyed $Zn_xCd_{1-x}S$ nanocrystals with highly narrow luminescence spectral width, Journal of the American Chemical Society 125 (2003) 13559–13563.

[15] Y.J. Hsu, S.Y. Lu, Y.F. Lin, One-step preparation of coaxial CdS–ZnS and $Cd_{1-x}Zn_xS$–ZnS nanowires, Advanced Functional Materials 15 (2005) 1350–1357.

[16] S.N. Garaje, S.K. Apte, S.D. Naik, J.D. Ambekar, R.S. Sonawane, M.V. Kulkarni, A. Vinu, B.B. Kale, Template-free synthesis of nanostructured $Cd_xZn_{1-x}S$ with tunable band structure for H_2 production and organic dye degradation using solar light, Environmental Science and Technololgy 47 (2013) 6664–6672.

[17] M. Dash, F. Chiellini, R.M. Ottenbrite, E. Chiellini, Chitosan—a versatile semi-synthetic polymer in biomedical applications, Progress in Polymer Science 36 (2011) 981–1014.

[18] T.H. Silva, A. Alves, B.M. Ferreira, J.M. Oliveira, L.L. Reys, R.J. F. Ferreira, R.A. Sousa, S.S. Silva, J.F. Mano, R.L. Reis, Materials of marine origin: a review on polymers and ceramics of biomedical interest, International Materials Reviews 57 (2012) 276–307.

[19] H.V. Sæther, H.K. Holme, G. Maurstad, O. Smidsrød, B.T. Stokke, Polyelectrolyte complex formation using alginate and chitosan, Carbohydrated Polymers 74 (2008) 813–821.

[20] J. Koetz, J. Baier, S. Kosmella, Formation of zinc sulfide and hydroxylapatite nanoparticles in polyelectrolyte-modified microemulsions, Colloid and Polymer Science 285 (2007) 1719–1726.

[21] W.B. Tan, N. Huang, Y. Zhang, Ultrafine biocopatible chitosan nanoparticles encapsulating multi-coloured quantum dots for bioapplications, Journal of Colloid and Interface Science 310 (2007) 464–470.

[22] D.V. Petrov, B.S. Santos, G.A.L. Pereira, C.M. Donegá, Size and band-gap dependences of the first hyperpolarizability of $Cd_xZn_{1-x}S$ nanocrystals, Journal of Physical Chemistry B 106 (2002) 5325–5334.

[23] A.A. Bol, R.V. Beek, A. Meijerink, On the incorporation of trivalent rare earth ions in II–VI semiconductor nanocrystals, Chemistry of Materials 14 (2002) 1121–1126.